ORIGINAL ARTICLE

Synthesis and characterization of nanocelluloses isolated through acidic hydrolysis and steam explosion of *Gliricidia sepium* plant fiber

Febiya Anna Fedin[1] · Harsha Mohan[1] · Sabu Thomas[2] · Jayachandran Kochupurackal[1]

Abstract

The exploration of cheaper sources of lignocellulosic biomass as raw material in nanocellulose production is the need of the time. The present study investigate the potential of a novel, abundant, and environmentally under-utilized plant-*Gliricidia sepium* for the extraction of nanocelluloses. Both cellulose nanofibers (CNFs) and cellulose nanocrystals (CNCs) were successfully isolated from *G. sepium* fibers (GS fibers). The synthesized nanocelluloses and the untreated raw fibers obtained were subjected to various characterization technologies, viz., field emission scanning electron microscopy (FE-SEM), transmission electron microscopy (TEM), Fourier transform infrared analysis (FTIR), thermogravimetric analysis (TGA), X-ray diffraction analysis (XRD), and zeta potential analysis. CNCs and CNFs had an aspect ratio of 38.29 and 148.65, respectively. Thermal stability was higher for CNC with a major degradation peak at 335 °C, whereas for CNF, it was 230 °C, and for raw fibers, it was 62 °C. The crystallinity index (CI) of the samples were found in the order of CNC (75%) > CNF (70.9%) > raw fibers (62.4%). Zeta potential measurements showed high negative value, − 51.0 mV for CNC and − 68.5 mV for CNF. High aspect ratio, crystallinity index, and zeta potential value along with better thermal stability traits of the nanocelluloses extracted from GS fibers make it a novel adaptable material for reinforcements in nanocomposite fabrication.

Keywords Nanocelluloses · Crystallinity index · *Gliricidia sepium* · Aspect ratio · Thermal stability

1 Introduction

Today, the environmental ecosystem is significantly distressed and compromised due to the widespread use of non-biodegradable petroleum-based products. In 2019, global plastic production amounted to 368 million metric tons (Mt) and is predicted to double within the next 20 years. Most of these products are designed for single use, with limited recyclability that has resulted in increased global production and unprecedented waste generation [1]. In this regard, future materials should align with the principles of circular economy, where resources are utilized in a sustainable and regenerative manner, promoting a closed-loop system that minimizes waste and environmental impact. The concepts of sustainable development and circular economy lead to growing trend of replacing synthetic materials with nature-derived materials and bio-based products [2].

Amongst all the bio-based polymers, cellulose stands out as the most abundant in the biosphere, predominantly present in algae, plants, fungi, tunicates, and bacteria. Cellulose is a linear polysaccharide linked by β-1,4-glycosidic bonds, having molecular formula $(C_6H_{10}O_5)_n$, where n represents the number of β-glucose monomers. Nanocelluloses isolated from cellulose with dimensions ranging from 1 to 10 nm outperform the native cellulose fibers and have drawn researcher's interests due to the unique characteristics they endow such as high crystallinity, low density, high surface area, low coefficient of thermal expansion, high purity, unique optical properties, mesh like entangled structures and high Young's modulus [3]. There are two types of plant-derived nanocelluloses—cellulose nanocrystals consisting needle like particles with high crystallinity and cellulose nanofibers with long thread/network like structure [4].

✉ Jayachandran Kochupurackal
jayachandrank@mgu.ac.in

1 School of Biosciences, Mahatma Gandhi University, P. D .Hills, Kottayam 686560, Kerala, India

2 IIUCNN, Mahatma Gandhi University, P. D .Hills, Kottayam 686560, Kerala, India

Cellulose fibrils are aligned along the length of the fiber, embedded in lignin/hemicellulose matrix, and therefore, lignocellulosic fiber is referred to as naturally occurring composites. As the components in plant fibers include cellulose, lignin, hemicellulose, and few amounts of pectins and waxes, the fibers should be pretreated to isolate cellulose molecules which include alkali treatment and bleaching. The most frequently used method for the extraction of CNCs is acid hydrolysis, which can disrupt the hydrogen bonds and cleave the amorphous domains of fibers to yield crystalline particles. Steam explosion process is a promising technique for CNF extraction. It is a thermomechanical process where the fiber pulp is exposed to pressurized steam for short periods of time, followed by the rapid release of pressure, causing the rupture of fiber cell wall and its defibrillation [5].

Nanocelluloses, because of their renewable and sustainable nature, remarkable mechanical strength and biodegradability, represent a promising solution for addressing various challenges in industries ranging from packaging, textiles, and biomedical and environmental sectors. Some of the applications of nanocelluloses include biological-based packaging, superabsorbent soil hydrogel, bone and cartilage tissue engineering, controlled release combo hydrogel for sustainable agriculture, and aerogel for oil spill treatments [6–8]. Recently, a lot of studies related to nanocelluloses focus on the development of biodegradable biomedical materials, that includes electrospun nanofiber membranes, nanocellulose-based aerogel and hydrogel, nanocellulose-based scaffolds, nanocarriers in cancer therapy, and biologically responsive nanomaterials for biosensing. Nanocelluloses are biocompatible, biodegradable, and versatile and can be engineered to have controlled porosity, surface chemistry, and mechanical properties, holding tremendous promise in biomedical field [9–11]. The effective incorporation of biomass nano pigment into cotton fabric offered a novel approach for the sustainable application of cellulose fibers, creating fabrics that are not only colored efficiently but also functional with qualities such as durability, UV resistance, and antibacterial properties [12]. These applications underscore the potential of nanocelluloses across diverse sectors, showcasing their significant role in driving advancements in material science, sustainability, and technological innovation.

Gliricidia sepium, commonly called "Mexican lilac," is a medium-sized legume tree native to Central America and belonging to the Fabaceae/Leguminosae family, the third largest family in the plant world [13]. Its leaves exhibit a range of beneficial properties. They possess anthelmintic effects, contain flavanoids, saponins, and tannins acting as anti-inflammatory agents, and promote wound healing. It also exhibits caffeine removal and coir pith detoxification properties [14]. The plant has fibrous stem, which contributes to its strength and resilience and can be regarded as a potential source of fiber for various industries. But the source remains entirely unexplored for nanocellulose production, offering significant research opportunity in this field. Exploring the economic viability of harnessing the barks of this plant for cellulose and nanocellulose synthesis steps can be now undertaken to transform discarded waste into a value-added product, thereby mitigating pollution linked to traditional waste disposal methods.

The goal of this work is to extract cellulose and synthesize both CNFs and CNCs from GS fibers, which will serve as a blueprint for the exploration of other under-utilized plants. This study investigated the potential of using GS fibers as a novel and alternative source of nanocelluloses through a series of processes, commencing with the separation of GS fibers from the bast portion of plant, removal of non-cellulosic components using chemical pre-treatments, and nanocellulose production via acid hydrolysis, steam explosion, and high pressure homogenization. TEM, FE-SEM, AFM, FTIR, XRD, TGA, and zeta potential measurements were used to comprehensively characterize the nanocelluloses to provide information on its morphology, size, shape, chemical structure, crystallinity, thermal stability, thermal decomposition rate, surface charge, and colloidal stability.

2 Materials and methods

2.1 Feedstock and chemicals

The raw material used for the current study was *Gliricidia sepium* fibers. The samples were collected from a household plantation in Alappuzha district of Kerala. Sodium hydroxide, glacial acetic acid, sodium hypochlorite, citric acid, and sulfuric acid are procured from Sigma-Aldrich, Merck, and HiMedia.

2.2 Cellulose extraction from GS fibers

The bast portion of the plant was separated and submitted to water retting by submerging it in an adequate volume of water to completely cover the entire basts. After complete retting of the bast, the plant fibers were isolated, washed, dried, and grounded into powder. The non-cellulosic components in GS fibers were first eliminated to extract cellulose. This was performed by the application of alkali and bleaching treatment to reduce the amorphous content which includes hemicellulose and lignin. The alkali treatment was carried out by soaking the grounded fibers in 5% NaOH solution for overnight at room temperature, followed by heating at 70 °C for 2 h with mechanical stirring and then washed with water and dried. The alkali treated biomass was then bleached using bleaching mixture (Solution A—acetic acid, NaOH, and water and Solution B—sodium hypochlorite and water in the ratio 1:1). The biomass was soaked in

bleaching mixture, heated at 50 °C for 1 h, washed to neutral, and continued till the biomass attained a white color [15]. The bleached fibers were sealed and stored at 4 °C.

2.3 CNC and CNF isolation from GS fibers

CNCs were prepared from GS fibers via the acid hydrolysis process. The bleached fibers were hydrolyzed using 65 wt% sulfuric acid at 45 °C for 30 min. Concentrated sulfuric acid was slowly added to the fiber placed in a beaker surrounded by ice-packs with thorough mixing and then kept at 45 °C for 30 min in a hot plate magnetic stirrer. After the treatment, the suspension was poured into 10-fold volume of water to stop the hydrolysis reaction. It was centrifuged at 3000 and subsequently at 12,000 rpm for 15 min each. The residue after centrifugation was subjected to dialysis for the removal of excess acid and was homogenized at 8000 rpm for 2 h [15]. CNFs were synthesized by means of steam explosion technique. Bleached fibers were immersed in 45% citric acid and allowed to attain 15 lbs pressure at 120 °C in steam explosion unit. Then, the pressure was released rapidly. The steam exploded fibers were then dialyzed against distilled water of pH 7 to obtain neutral fibers. Following this, the fibers were homogenized using IKA T25 Digital ULTRA TURRAX high pressure homogenizer at 8000 rpm for 2–3 h [16].

2.4 Nanocellulose characterization

2.4.1 Morphological analysis

Morphological analysis and surface characterization of CNCs and CNFs extracted from GS fibers were undertaken by TEM, SEM, and AFM analysis. For TEM analysis, an aqueous solution of both nanocelluloses was deposited on carbon-coated grids and then observed with TEM (JEOL JEM 2100 Lab6 type) operating at 200 kV. The size analysis was done by ImageJ software, and 20 TEM images were taken for each sample. The nanocellulose solution stored at 4 °C along with raw, alkali-treated, and bleached fibers were observed using FE-SEM (MAIA3 XMH TESCAN) operating at 5.0 kV and scanning electron microscope (JEOL – JSM – 6390) operating at 10 kV. The fiber samples were initially dropped on a carbon coated tape and dried at atmospheric temperature. The dried samples were coated with gold by an ion sputter coater and then observed. AFM imaging was carried out in confocal Raman microscopy coupled with AFM (WITec ALPHA 300RA) instrument. All imaging was done in non-contact mode using a silicon tip of 75.0 kHz resonant frequency, 2.80 N/m force constant, and a radius less than 8.00 nm. The samples were prepared on a fresh mica sheet, dried under a gentle steam of nitrogen gas, and subjected to AFM study.

2.4.2 Chemical composition analysis

The chemical composition of GS fibers at each stage of treatment was determined by the protocol described by Ramadevi et al. (2012) [17]. Yield of GS nanocelluloses were noted using the following equation.

$$\text{Yield \%} = (W1/W0) * 100 \tag{1}$$

where $W0$ is the weight of GS raw fibers and $W1$ is the weight of nanocelluloses obtained (dried) [18].

2.4.3 FTIR analysis

FTIR spectra were obtained using a PerkinElmer spectrum two IR version 10.6.0. The sample spectra were recorded in the wavenumber range 4000–400 cm^{-1}. The raw GS fibers, alkali-treated, bleached, and nanocelluloses synthesized underwent FTIR analysis.

2.4.4 Thermogravimetric analysis

The thermal stability and degradation of nanocelluloses and untreated raw fibers obtained were performed using a thermal analyzer (SDT Q600 V20.9 Build 20). Required amount of sample was heated till 700 °C under a N2 atmosphere with a flow rate of 99 ml/min. The thermograms of nanocelluloses were compared with that of raw GS fibers.

2.4.5 X-ray diffraction analysis

X-ray diffraction analysis of the nanocelluloses and raw fibers were performed with Rigaku Miniflex 600 with CuKα1 as the source and 1.5406 A° as the source wavelength (λ) operating at 40 kV and 13 mA. The detection was carried out using a 2θ scan from 10 to 90°. The sample was filled in a glass slide for analysis. The crystallinity index (CI) of the nanocelluloses was calculated from the heights of the 002 peak (I002, $2\theta = 22.6°$) and the intensity minimum between the 002 and 101 peaks (Iam, $2\theta = 18°$) using the Segal equation [19] as described in Eq. 2.

$$\text{Crystallinity Index, CI} = \frac{[I002 - Iam]}{I002} \times 100 \tag{2}$$

where $I002$ is the diffraction intensity close to $2\theta = 22$ and represents a crystalline material; Iam is the diffraction intensity close to $2\theta = 18$ and refers to amorphous material in cellulosic fibers.

### 2.4.6 Zeta potential analysis

Stability of nanocellulose suspensions were determined using zeta potential measurements. It was measured with a nanoparticle analyzer (HORIBA SZ-100) having DPSS LASER 532 nm as the light source. Aqueous suspensions of the samples kept at 4 °C were used for the measurement.

3 Results and discussion

Environmentally undesirable and profusely growing biomass source like *G. sepium* utilized for a sustainable promoting process is the key attraction of the study. The plant can be regarded as a profound source for nanocellulose isolation for its novelty value and untapped potential. The cellulose fibers were successfully isolated via a sequential process of water retting, alkaline treatment, and bleaching. The extraction procedures and their corresponding outcomes are depicted in Fig. 1. The bleached GS fibers were then used for CNC and CNF preparation. Visual analysis of the fibers was conducted at each step. Discoloration of the fiber after each treatment was noticed as gradual change from creamish

white for the initial retted fibers, yellow for the alkali treated fibers, and pure white for the bleached fibers. Acid hydrolysis and steam explosion resulted in the formation of CNCs and CNFs, respectively, with a white color. The dark color observed in the fiber is attributed to the presence of lignin and impurities. These impurities are effectively removed through pretreatments, resulting in a lighter coloration of the fibers [18]. Water retting conducted for 2 weeks resulted in the complete separation of bast fibers, which were then washed with tap water and oven-dried. Water retting was followed by alkaline treatment resulting in partial removal of the binding materials like hemicelluloses, lignin, pectin, wax, and other impurities. The fibrillation of GS fibers is attributed to the alkali treatment as it helps in breaking the linkage of hemicellulose and lignin complex [20]. These effective pre-treatments resulted in the disintegration of lignin, cellulose, and hemicellulose complex.

The key factors influencing the extraction efficiency of nanocelluloses from GS fibers are the duration and concentration of pre-treatments, optimal steam explosion cycle (5–8), ideal acid hydrolysis conditions (65 wt% H_2SO_4 at 45 °C for 30 min) and high pressure homogenization for 2–3 h. Higher temperatures and longer processing time can
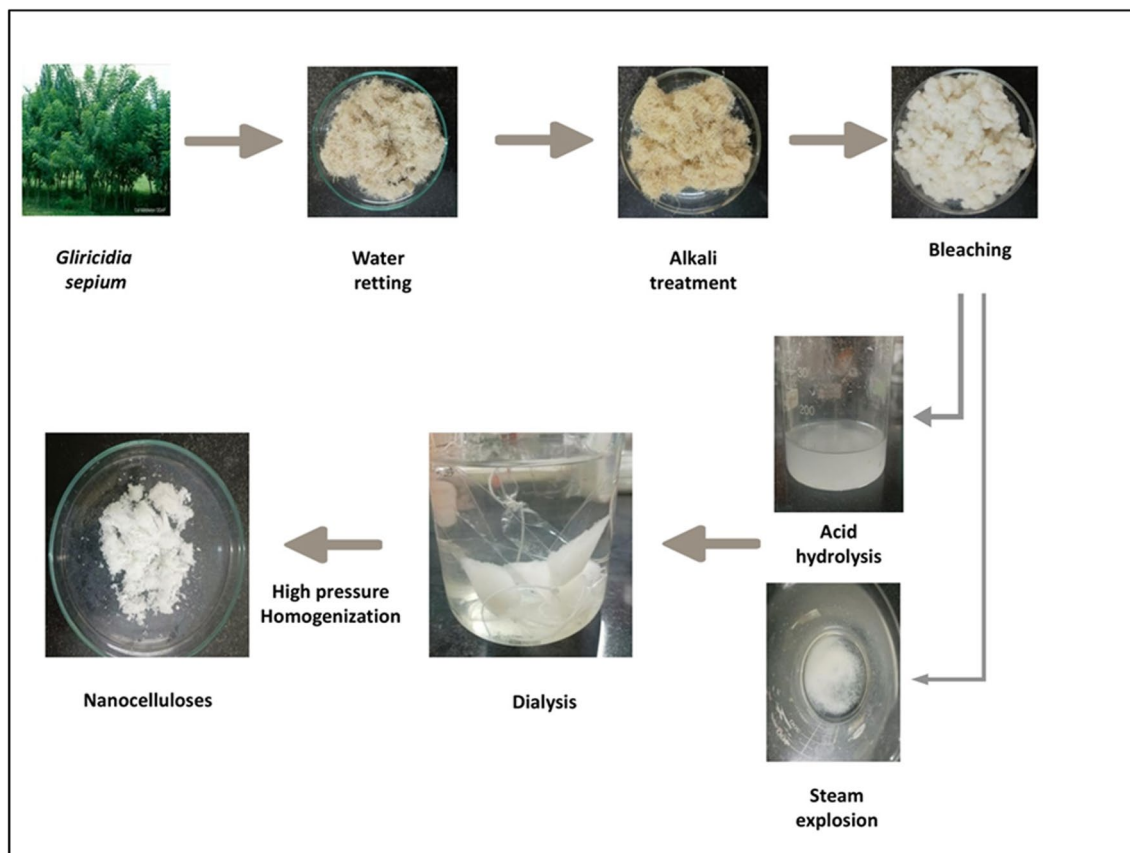
Fig. 1 The schematic representation of different stages in the preparation of nanocelluloses from *Gliricidia sepium*

accelerate the breakdown of bond between cellulose and lignin/hemicellulose complex due to increased reaction rates and extensive interaction. However, they can also result in cellulose degradation and side reactions. Therefore, finding an optimal balance between temperature and time is crucial for cellulose and nanocellulose production efficiency. The main challenges encountered while extracting nanocelluloses from GS fibers are the following:

i.   Limited understanding

The lack of prior research on utilizing *Gliricidia sepium* as a source for nanocellulose extraction posed a challenge, as it led to uncertainties regarding nanocellulose yield and a dearth of knowledge regarding its chemical composition.

ii.   High hemicellulose content

Hemicellulose is a complex polysaccharide that is closely associated with cellulose and other components in plant cell wall. Its efficient removal is required for cellulose purification. This was achieved through the application of high concentrations of chemicals (5% NaOH, 45% citric acid, 65 wt% H_2SO_4) and by increasing the cycles of specific chemical treatments.

iii.   Unpleasant odor

Gliricidia sepium possesses an inherent unpleasant odor arising from the presence of various components within the plant tissues, e.g., saponins, alkaloids, and organic acids. This presents a challenge, particularly during plant collection and processing activities like retting.

3.1 Microscopical analysis

The SEM micrographs of raw GS fibers were found to be intact and smooth, and without any structural deformations, this can be attributed to the outer non-cellulosic layer composed of lignin, hemicelluloses, pectin, wax, and oil. The subsequent pre-treatments lead to the successful elimination of non-cellulosic impurities which is understood from the SEM images of alkali-treated and bleached fibers. TEM and FTIR analysis provided additional substantial evidence for the removal of amorphous component. Nanocelluloses synthesized had a distinct morphology and much reduced diameter. Figure 2 shows the SEM micrographs of raw GS fibers and alkali-treated and bleached fibers.

Figure 3 represented the SEM, TEM, and AFM images of CNCs and CNFs synthesized from GS fibers. The morphology and dimension of CNCs and CNFs varied each other. CNCs had short rod shaped structures which are slightly aggregated at some fields of microscopy, showing similarity with the CNCs extracted from poplar wood via sulfuric acid hydrolysis [21]. CNCs had an average length of 235.887 nm and diameter of 6.16 nm. Acid hydrolysis of celluloses resulted in the hydrolytic cleavage of glycosidic bonds between two anhydroglucose units and dissolution of amorphous part leaving behind the crystalline regions. Mechanical treatment like high pressure homogenization following acid hydrolysis lead to the disintegration of cellulose structure to nanocrystalline cellulose particles. CNFs synthesized exhibited web-network structures with long entangled nanofibrils having an average diameter of 6.81 nm. The length of nanofibrils were difficult to calculate
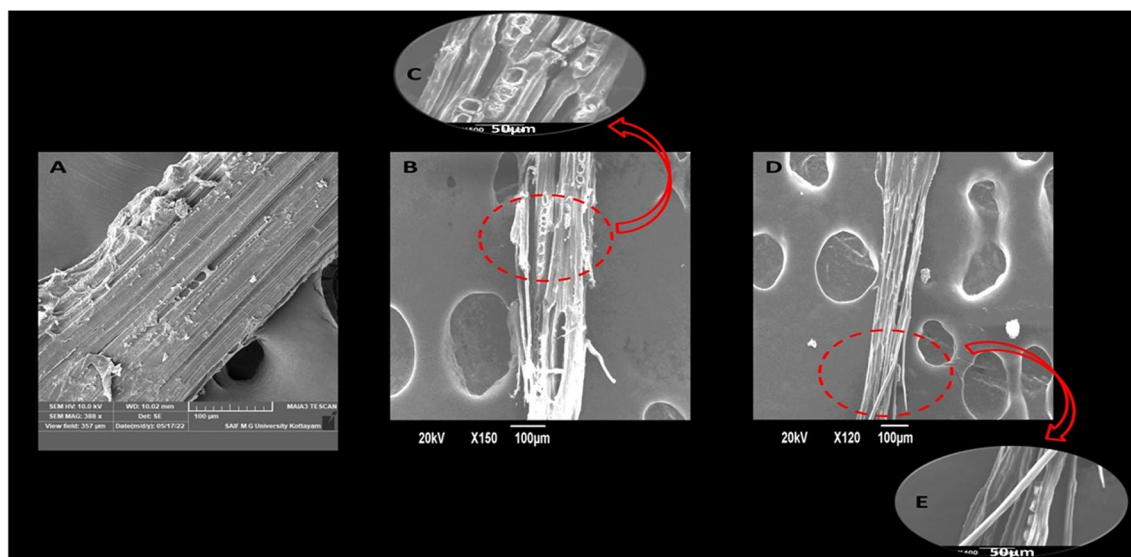
Fig. 2 SEM images of **A**, **B**, **D** raw GS fibers and alkali-treated and bleached fibers in 100-μm scale, respectively. **C**, **E** Alkali-treated and bleached GS fibers in 50-μm scale

Fig. 3 Microscopical analysis. **A–D** SEM, TEM, AFM, and suspension of CNC. **E–H** SEM, TEM, AFM, and suspension of CNF
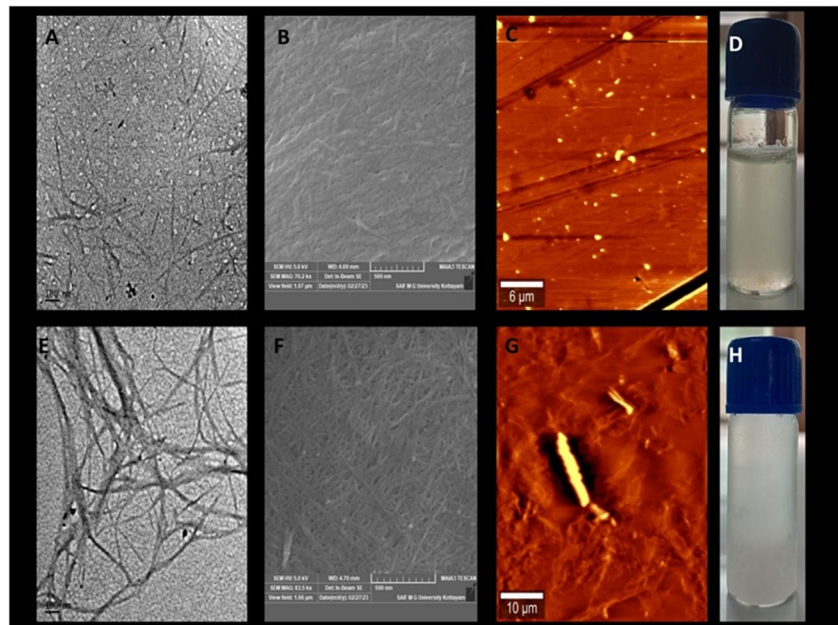
Table 1 Size distribution of CNC and CNF from TEM measurement (calculated using ImageJ software)

Samples	Length (L, nm)	Diameter (D, nm)	Aspect ratio L/D
CNC	235.887	6.16	**38.29**
CNF	On an average greater than 1012.321	6.81	On an average greater than **148.65**

Table 2 Chemical composition of GS fiber at each stage of nanocellulose preparation

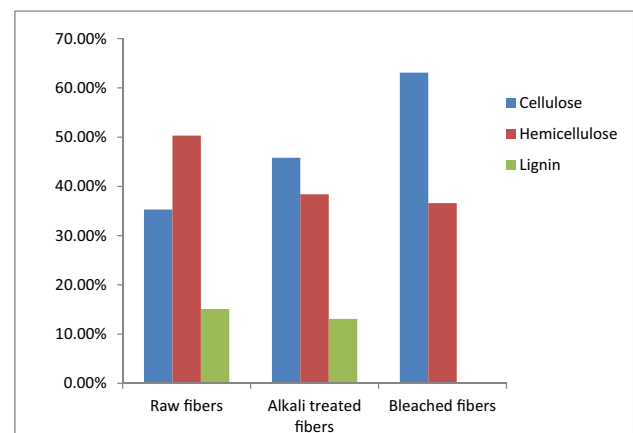| Fiber	Cellulose (%)	Hemicellulose (%)	Lignin (%)
Raw	35.3 ± 0.35	50.3 ± 1.04	15.1 ± 0.66
Alkali treated	45.8 ± 0.95	38.4 ± 1.22	13.1 ± 0.47
Bleached	63.1 ± 0.70	36.6 ± 0.94	0.14 ± 0.005

as they were very long, entangled, and overlapped structures; however, the average length was approximately greater than 1000 nm. Multiple and continuous steam explosion of bleached fibers in acid medium under high pressure lead to the conversion of microfibrils to nanofibrils. High shear forces developed during sudden pressure drop caused the defibrillation [20]. Table 1 summarized the size distribution and aspect ratios of nanocelluloses. It was apparent from the values that cellulose nanofibers were having high aspect ratio. Nanocelluloses with greater aspect ratios have potential advantages such as improved mechanical strength, enhanced reinforcement capability, increased surface area, and in developing high-performance materials [5]. AFM and SEM micrographs gave supporting evidence for the formation of nanocelluloses.

3.2 Chemical composition analysis and yield of nanocelluloses

The yield of *G. sepium* nanocelluloses was found to be 51.4% and could be considered as a potential source for nanocellulose production. The chemical composition of GS

Fig. 4 Trend in the chemical composition of GS fibers at each pre-treatment level

fibers at each level of pre-treatments was summarized in Table 2 and graphically represented in Fig. 4. It was evident from the percentage values that each successive treatment level marked an increase in the concentration of cellulose

and decrease in lignin and hemicellulose proportion. This was further supported by the evidences from FTIR results. The chemical composition of two other plants belonging to the same family Leguminosae, namely, *Acacia arabica* and *Cajanus cajan*, had similar values. The cellulose content in *Acacia arabica* were found to be 36.2% and *Cajanus cajan* had its lignin content near to 18% [22]. Table 3 gives a comparison on the chemical composition and nanocellulose yield of GS fibers with some of the traditional fiber sources.

3.3 Functional group analysis

FTIR spectrum of the extracted CNC and CNF was compared with that of raw fibers (Fig. 5a) and pure nanocelluloses (Fig. 5b). The band at 1457 cm^{-1} in the FTIR spectrum of raw fiber represented CH2 deformation stretching in lignin/xylan and the peak at 1732 cm^{-1} represented C=O stretching of the acetyl and uronic ester groups of pectin/hemicellulose/ester linkage of carboxylic groups of ferulic acid in lignin [32]. One small peak 2857 cm^{-1} is attributed to the C-H stretching of hemicellulose [33]. The peaks at 1102 cm^{-1} and 1027 cm^{-1} is related to C-O-C stretching and C-OH stretching of lignin, respectively [34]. The peak between 1300 and 1200 cm^{-1} depicts an out of plane C-O stretching in the aryl group of the lignin [32]. These specific peaks were reduced in the spectra of nanocelluloses confirming the removal of hemicellulose and lignin components.

A wide band between 3400 and 3200 cm^{-1} in the FTIR data of nanocelluloses extracted typically represented the stretching vibrations of the hydroxyl (-OH) groups present in the cellulose structure [16]. This region is referred to as one of the most prominent features in the FTIR spectrum of cellulose-based materials. This peak narrows following extraordinary treatments, suggesting the removal of some amorphous components. The bands in nanocelluloses near 1050 and 1057 cm^{-1} were associated with the C-O
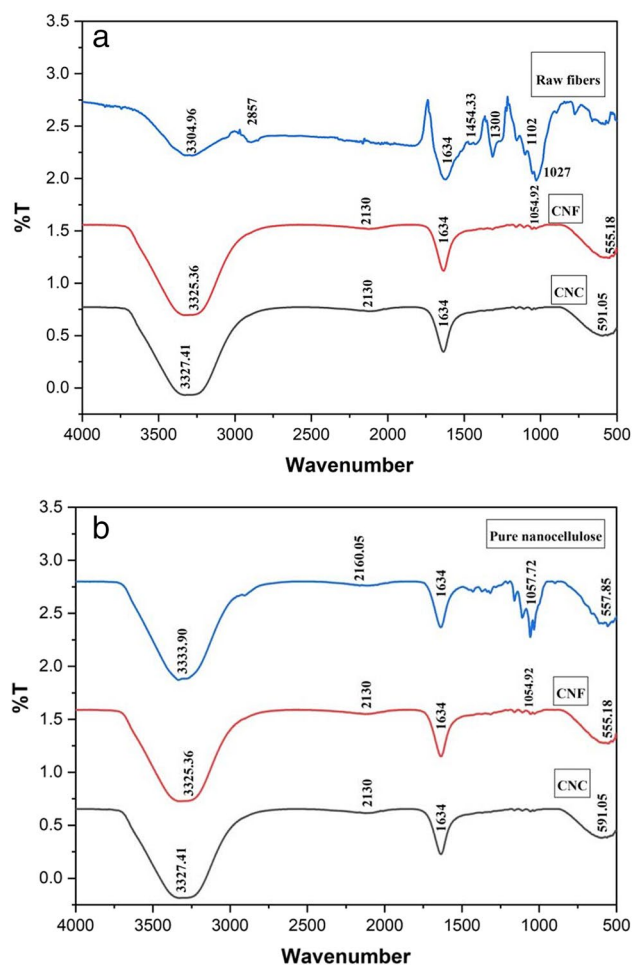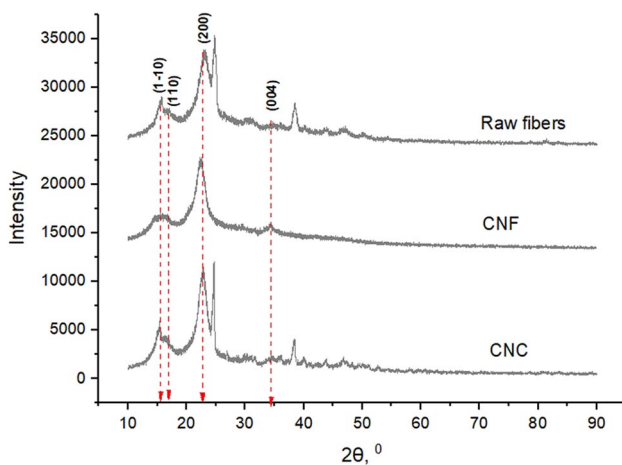

Fig. 5 FTIR spectrum analysis. **a** FTIR spectra of raw GS fibers with nanocelluloses extracted. **b** FTIR spectra of extracted nanocelluloses with pure nanocellulose

Table 3 Chemical composition and yield of GS fibers with some of the traditional fiber sources [23]

Sl. No.	Fiber source	Cellulose (%)	Hemicelulose (%)	Lignin (%)	Nanocellulsoe/cellulose yield (%)	References
1	Jute bast	62.1	21.8	14.0	50.5	[24]
2	Ramie	69.83	9.63	3.98	89.35	[25]
3	Cotton	> 95	-	0.08	89.9	[26]
4	Oil palm empty fruit bunch	44.4	30.9	14.2	> 80	[27]
5	Sugarcane bagasse	44.55	21.81	22.52	63.5	[23]
6	Pineapple leaf	81.27	12.37	3.46	40.1	[28]
7	Coconut coir	39.3	2	49.2	40	[29]
8	*Urtica dioica*	41.7	18.4	19.2	88	[30]
9	*Acer platanoides*	60–70	10–11	8–9	70	[18]
10	*Alstonia scholaris*	50.3	9.3	7.7	70	[31]
11	***Gliricidia sepium* bast**	**35.3**	**50.3**	**15.1**	**51.4**	**Present work**

Table 4 FTIR peak positions, corresponding functional groups, and chemical constituent in the GS fiber and nanocelluloses extracted

Peak positions (wavenumber, cm^{-1})	Functional group	Chemical constituent	Reference
1457	CH2 stretching	Lignin	[32]
Peak between 1300 and 1200	C-O stretching	Lignin	[32]
1102	C-O-C stretching	Lignin	[34]
1027	C-OH stretching	Lignin	[34]
1732	C=O stretching	Hemicellulose	[32]
2857	C-H stretching	Hemicellulose	[33]
Wide band between 3400 and 3200	O-H stretching	Cellulose	[16]
1057	C-O stretching and vibration	Cellulose	[21]
1050	C-O stretching and vibration	Cellulose	[21]
550	C-O-C glycosidic bond	Cellulose	[35]
2130	Presence of -COO$^-$ and C-O groups	Cellulose	[36]
1634	O-H bending	Adsorbed water molecule	[16]

Fig. 6 XRD spectra of raw GS fibers and nanocelluloses extracted

Table 5 Crystallinity index of raw fiber and its nanocelluloses

Samples	I200	Iam	CI (%)
Raw fibers	8500.00	3191.67	62.4
CNF	9616.67	2791.67	70.9
CNC	10,633.33	2658.33	75.0

3.4 XRD analysis

The raw fibers and nanocelluloses synthesized were dried to powder form and subjected to XRD analysis to investigate their crystalline behavior. The XRD graphs of all the samples are shown in Fig. 6. All the diffractograms exhibited two significant peaks that represented the typical cellulose I structure, peaks around $2\theta = 16.5°$ and 22.6° corresponding to the (101), and (200) crystal planes of cellulose crystalline structure, respectively [31]. The height of the intensity minimum between the (200) and the (101) peaks ascribed to the amorphous wood regions (Iam) and the width and intensity of the peaks at $2\theta = 16.5°$ and 22.6° represented the relative crystallinity of the samples [37]. The crystallinity index (CI) of the three samples were calculated by Segal's equation and the CI values obtained were 75, 70.9, and 62.4% for CNC, CNF, and raw fibers, respectively. Table 5 provided the detailed information on the crystallinity indices of the samples.

In a lignocellulosic fiber, hemicelluloses and lignin are the amorphous constituents whereas cellulose constitutes the crystalline structure due to the presence of inter- and intra-hydrogen bonding and van der Waals forces between the adjacent molecules. Raw fiber owns the highest percentage of lignin and hemicellulose and hence has the lowest crystallinity. The intensity of peaks at $2\theta = 16.5°$ and 22.6° was relatively high for the acid treated cellulose nanocrystals. The increased crystalline nature of nanocrystals is due to

stretching and vibration of pyranose ring skeletal in the cellulose backbone, respectively [21]. The peak observed near 550 cm^{-1} in the FTIR spectrum was ascribed to the bending vibrations of C-O-C glycosidic bond in the cellulose molecule [35]. The presence of carboxylate groups (-COO-) and carbonyl groups (C=O) could be inferred from a broad absorption band near 2130 cm^{-1} [36]. These groups could be formed in the fiber through the application of various chemical treatments, especially acid hydrolysis. Moreover, these bands were in good agreement with the commercial nanocellulose purchased from Sappi Maastricht Mill, The Netherlands.

The peak at 1634 cm^{-1} could be attributed to the OH bending of adsorbed water molecules [16] and might be adsorbed on the surface of nanocellulose particles. The FTIR peak position, its corresponding functional groups, and chemical constituent of GS fiber and nanocelluloses extracted are listed in Table 4.

the more efficient elimination of non-cellulosic components and dissolution of amorphous zones [20]. In the process of acid hydrolysis, the hydronium ions get penetrated the cellulose chains targeting vulnerable amorphous regions and accelerates the hydrolytic cleavage of the glycosidic bonds, ultimately leading to the release of individual crystallites over time. The high crystallinity index of CNCs indicates that their cellulose chains are tightly packed together in an ordered manner [38]. The CI values of nanocelluloses as given in Table 5 showed 13–20% enhancement when compared to the raw, untreated fibers. A comparison on the crystallinity indices and nanocellulose extraction process of various plant sources is presented in Table 6.

3.5 Thermogravimetric analysis (TGA)

Figures 7 and 8 showed the TGA and its differential thermal analysis (DTA) graphs for raw fiber and nanocelluloses synthesized. The percentage of weight loss vs. temperature graph displayed three main weight loss regions for the samples (Fig. 7). The first region (region I) falling in the range of 20–100 °C was mainly due to the vaporization of free and bound water present in the sample. Region II ranging from 100 to 380 °C depicted a sharp weight loss,
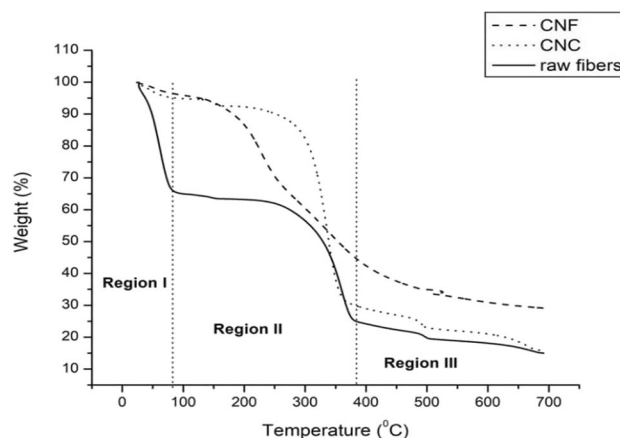

Fig. 7 Weight loss regions of raw GS fibers and nanocelluloses extracted

analogous to a dominant peak on the DTA curves, representing the main pyrolysis step of the analyzed samples. In region III, the less significant weight loss rate could be attributed to the oxidation and breakdown of char residue into low molecular weight gaseous products [46].

Table 6 A comparison on the crystallinity indices and nanocellulose extraction process of various plant sources

| Sl no.	Source	CNF extraction method	CI of CNF (%)	CNC extraction method	CI of CNC (%)	References
1	Jute bast	Multistage mechanical disintegration process (rotor-stator homogenizer, high-pressure homogenizer, ultrasonication)	67.54	Acid hydrolysis using 64% H_2SO_4	75.56	[39]
2	Pineapple leaf	Mild acid hydrolysis using 11% $H_2C_2O_4$	75.38	Acid treatment using 64% H_2SO_4	84.34	[28]
3	Bamboo	Microwave liquefaction combined with chemical treatment and ultrasonic nanofibrillation	67.4	Acid treatment using 64 wt% H_2SO_4	87	[40, 41]
4	Ramie	Chemical-ultrasonication treatment	73.65	Acid hydrolysis using 58 wt% H_2SO_4	90.77	[25, 42]
5	Banana pseudostem	Sonication using ultrasonic processor	87.5	Acid treatment using 64 wt% H_2SO_4	95.6	[43]
6	*Prosopis julifera*	Mechanical fibrillation using an ultrafine friction grinder	70.8	Acid treatment using 64 wt% H_2SO_4	76.3	[44]
7	Coir	Mild TEMPO-mediated oxidation and ultrasonication	56.3	Acid treatment using 60% w/w of H_2SO_4	68	[29, 45]
8	Rice straw	High pressure grinding with a super mass collider	54.4	Acid treatment using 64 wt% H_2SO_4	68	[21]
9	Poplar wood	High pressure grinding with a super mass collider	56.4	Acid treatment using 64 wt% H_2SO_4	72.9	[21]
10	***Gliricidia sepium* bast**	**Steam explosion using 45% citric acid followed by high-pressure homogenization**	**70.9**	**Acid treatment using 64 wt% H_2SO_4**	**75**	**Present work**
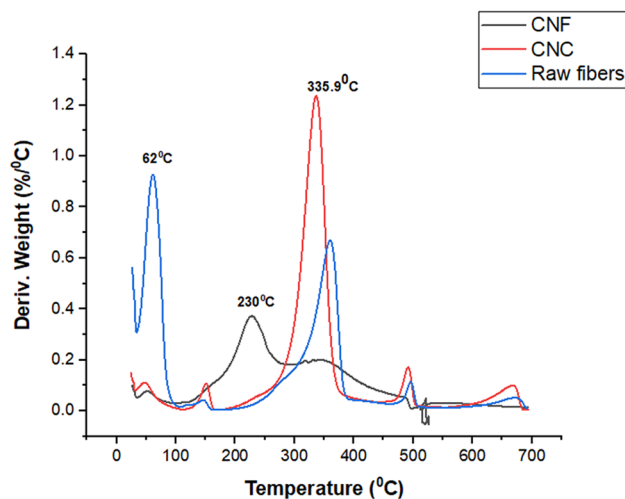
Fig. 8 DTA analysis of raw fibers and extracted nanocelluloses

For raw fiber, a sharp weight decline in TGA and a dominant peak in DTA in the region I corresponded to the evaporation of water. Lignocellulosic fibers are hydrophilic in nature due to the prevalent presence of hydrophilic compounds like cellulose, hemicellulose, and lignin molecules. This property stems from the numerous hydroxyl (-OH) groups, which can form hydrogen bonds with water molecules [5]. The next weight loss region for raw fiber (region II) fell in the range of 150–380 ℃, indicating the thermal degradation of hemicellulose, lignin, and the breakup of cellulose glycosidic linkages [47]. In the case of nanocelluloses obtained, region I did not illustrate a sharp weight loss which was attributable to the less hydrophilic nature of them when compared to the raw fiber. Higher crystallinity and the structural and chemical changes that occur during the processing steps were found

to be the main reasons behind this character. Region II in the TGA curves of CNC demonstrated a higher thermal stable nature. A high degradation occurred after 290 ℃, and more than 80% of its weight was stable by that stage. Considering region II of CNF, it presented a gentle decomposition rate. Eighty-eight percent of the total weight was retained till 200 ℃, and then, the graph softly lowered. Though CNF had reduced thermal stability than CNC, it still demonstrated greater stability than raw fibers. This could be validated from the obtained TGA curves. Upon examining the TGA curves, it was observed that at 315 ℃ (the temperature at which raw fiber experiences rapid weight loss in region II), the raw fiber had retained only 50% of its original weight, while CNF had retained 60% of its weight. DTA of raw fibers, CNF, and CNC shows major degradation peaks around 60 ℃, 230 ℃, and 335 ℃, respectively, which is depicted in Fig. 8.

Hence, the thermal stability of the samples followed the order of CNC > CNF > raw fibers. This is due to the fact that untreated fibers are composed of long cellulose chains or fibrils, which is surrounded by high concentration of lignin, hemicellulose, pectin, and other impurities. These chemical components may create additional active sites and accelerate the onset of thermal degradation, causing the raw fiber to degrade earlier than nanocelluloses obtained [20]. Trache et al. 2020 [48] in their studies on thermal analysis of lignocellulosic fibers reported that the higher thermal stability of nanocelluloses was the result of complete removal of hemicelluloses and lignin. The enhanced thermal stability and poor hydrophilic nature of the nanocelluloses can be utilized in the production of nanocomposites. Moreover, the absence of any degradation in the conventional polymer processing temperature range below 200 ℃ was also advantageous.
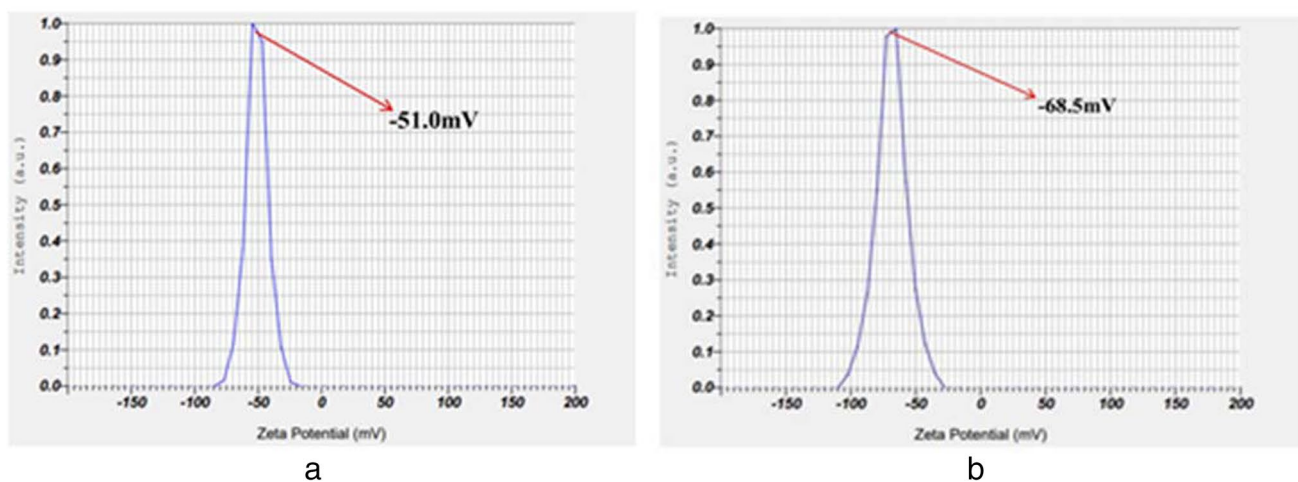
Fig. 9 Zeta potential measurements of nanocelluloses synthesized from raw GS fibers

Table 7 A comparison of the nanocelluloses synthesized from GS fibers

Sl. No.	Comparative parameters	CNCs	CNFs
1	Preparation	Via acid-hydrolysis and high pressure homogenization	Via steam explosion and high pressure homogenization
2	Morphological	Rod-like/needle-like particles	Thread-like bundles of cellulose chain with long, flexible, and entangled nanofibers
3	Length and diameter	Length in the range of 200 nm and diameter of less than 10 nm	Length in micrometer and diameter in nanometer range
4	Aspect ratio	Aspect ratio of 38.29	High aspect ratio (148.65)
5	Crystallinity	High crystallinity with CI of 75%	Crystalline with CI of 70%
6	Thermal stability	Thermally stable with major degradation peak at around 335 °C	Thermally stable with major degradation peak at around 230 °C
7	Colloidal stability	Colloidally stable with zeta potential of − 51.0 mV	Colloidally stable with zeta potential of − 68.5 mV

3.6 Zeta potential measurements

Zeta potential measurements were carried out on aqueous dispersions of the nanocelluloses extracted from GS fibers and represented in Fig. 9. Both of the cellulose suspensions, in distilled water, showed a negative zeta potential value, viz., CNC with a zeta potential value of − 51.0 mV (Fig. 9a) and CNF having − 68.5 mV (Fig. 9b). Zeta potential is defined as a measure of the stability of colloidal suspensions indicating the repulsion of similarly charged particles in a dispersion. Khouri in 2010 [49] reported that agglomeration of nanocelluloses occur between a zeta potential value of − 15 to 15 mV. Nanocellulose suspensions characterized by a high negative zeta potential value demonstrate excellent electrical and colloidal stability, making them ideal candidates for serving as effective reinforcing agents in polymer matrices [50]. The introduction of negatively charged sulfate and carboxylic groups during sulfuric acid hydrolysis and citric acid treatment enhances the stability of nanocellulose suspensions. In this sense, as in the present study, the nanocelluloses obtained from GS fibers have good colloidal stability and could be considered a good reinforcing material for bio-nanocomposite fabrication.

The results obtained such as high aspect ratio, crystallinity index, zeta potential value, and thermal stability of nanocelluloses extracted from *Gliricidia sepium* offer several advantages for their use in nanocomposite fabrication. Nanocelluloses with high aspect ratios provide effective reinforcement, improving mechanical properties such as stiffness, strength, and toughness by facilitating stress transfer within the composite matrix. Moreover, nanocelluloses with higher crystallinity indices exhibit stronger interfacial interactions with polymer matrices, resulting in improved compatibility, dispersion, and adhesion, leading to superior mechanical performance and stability of the nanocomposites. Additionally, the zeta potential value influences the dispersion and stability of nanocelluloses in polymer matrices during fabrication, with higher negative values ensuring more uniform dispersion and minimizing agglomeration. Furthermore, nanocelluloses with high thermal stability can withstand processing temperatures without significant degradation, maintaining the integrity of the composite structure and enhancing thermal properties. Collectively, these properties make nanocelluloses from *Gliricidia sepium* highly desirable for nanocomposite applications across various industries, especially in packaging and automotive applications.

The table given below (Table 7) does a comparison on the preparation and characteristics of the nanocelluloses (CNCs and CNFs) synthesized from GS fibers via the above mentioned methodologies and characterization technologies.

4 Conclusion

Gliricidia sepium is a medium-sized tree with lignocellulosic biomass, containing lignin, hemicellulose, and cellulose in various quantities. The chemical pre-treatments successfully intensified the cellulose content and made cellulose extraction possible. The SEM and FTIR analysis have supported the efficient extraction of cellulose by eliminating impurities. All the microscopical evidences and FTIR spectra confirmed the formation of CNCs and CNFs. The XRD analysis ratifies the presence of cellulose-I by the four significant peaks, with maximum crystallinity index reaching to 75%. The synthesized nanocelluloses were thermally stable, with highest thermal stability up to 335 °C, which is certified by the DTA and TGA graphs. Remarkable zeta potential measurements for nanocelluloses provide them with good electrical and colloidal stability. Altogether, the nanocelluloses synthesized from GS fibers proved to be a good candidate in bionanocomposite and biomaterial fabrication.

curation. Harsha Mohan: data curation, methodology, and resources. Sabu Thomas: supervision, writing—review and editing, and methodology. Jayachandran K.: supervision, funding acquisition, writing—review and editing, project administration, and conceptualization.

Data availability All data generated and analyzed during this study are included in the published article.

Declarations

Competing interests The authors declare no competing interests.

References

1. Walker TR, Fequet L (2023) Current trends of unsustainable plastic production and micro (nano) plastic pollution. TRAC Trends Anal Chem 160:116984. https://doi.org/10.1016/j.trac.2023.116984

2. Vahabi H, Jouyandeh M, Parpaite T, Saeb MR, Ramakrishna S (2021) Coffee wastes as sustainable flame retardants for polymer materials. Coatings 11(9):1021. https://doi.org/10.3390/coatings11091021

3. Rashid AB, Hoque ME, Kabir N, Rifat FF, Ishrak H, Alqahtani A, Chowdhury ME (2023) Synthesis, properties, applications, and future prospective of cellulose nanocrystals. Polymers 15(20):4070. https://doi.org/10.3390/polym15204070

4. Randhawa A, Dutta SD, Ganguly K, Patil TV, Patel DK, Lim KT (2022) A review of properties of nanocellulose, its synthesis, and potential in biomedical applications. Appl Sci 12(14):7090. https://doi.org/10.3390/app12147090

5. Deepa B, Chirayil CJ, Pothan LA, Thomas S (2019) Lignocellulose-based nanoparticles and nanocomposites: preparation, properties, and applications. In *Lignocellulose for future bioeconomy* (pp. 41–69). Elsevier. https://doi.org/10.1016/B978-0-12-816354-2.00004-9

6. Rizwan M, Gilani SR, Durani AI, Naseem S (2021) Materials diversity of hydrogel: synthesis, polymerization process and soil conditioning properties in agricultural field. J Adv Res 33:15–40. https://doi.org/10.1016/j.jare.2021.03.007

7. Rizwan M, Gilani SR, Durrani AI, Naseem S (2022) Kinetic model studies of controlled nutrient release and swelling behavior of combo hydrogel using Acer platanoides cellulose. J Taiwan Inst Chem Eng 131:104137. https://doi.org/10.1016/j.jtice.2021.11.004

8. Raghav GR, Nagarajan KJ, Palaninatharaja M, Karthic M, Ganesh MA (2023) Reuse of used paper egg carton boxes as a source to produce hybrid AgNPs-carboxyl nanocellulose through biosynthesis and its application in active food packaging. Int J Biol Macromol 249:126119. https://doi.org/10.1016/j.ijbiomac.2023.126119

9. Jiang Z, Han X, Zhao C, Wang S, Tang X (2022) Recent advance in biological responsive nanomaterials for biosensing and molecular imaging application. International Journal of Molecular Sciences, 23(3), 1923. https://doi.org/10.3390/ijms23031923

10. He X, Jiang Z, Akakuru OU, Li J, Wu A (2021) Nanoscale covalent organic frameworks: from controlled synthesis to cancer therapy. Chem Commun 57(93):12417–12435. https://doi.org/10.1039/D1CC04846E

11. Wang Y, Zhai W, Li J, Liu H, Li C, Li J (2023) Friction behavior of biodegradable electrospun polyester nanofibrous membranes. Tribol Int 188:108891. https://doi.org/10.1016/j.triboint.2023.108891

12. Zhang H, Fu R, Zheng Q, Song X, Wu J, Ren Y (2024) Continuous mode of color and functionality construction for cotton by bacterial pigment based on nano-suspension system. Ind Crops Prod 214:118510. https://doi.org/10.1016/j.indcrop.2024.118510

13. Grygier A, Chakradhari S, Ratusz K, Rudzińska M, Patel KS, Lazdiņa D, Górnaś P (2022) Seven underutilized species of the Fabaceae family with high potential for industrial application as alternative sources of oil and lipophilic bioactive compounds. Ind Crops Prod 186:115251. https://doi.org/10.1016/j.indcrop.2022.115251

14. Aulanni'am AA, Ora KM, Ariandini NA, Wuragil DK, Permata FS, Riawan W, Beltran MAG (2021) Wound healing properties of Gliricidia sepium leaves from Indonesia and the Philippines in rats (Rattus norvegicus). Veterinary World, 14(3)

15. Padinjakkara A, Scarinzi G, Santagata G, Malinconico M, Razal JM, Thomas S, Salim NV (2020) Enhancement of adhesive strength of epoxy/carboxyl-terminated poly(butadiene-*co*-acrylonitrile) nanocomposites using waste hemp fiber-derived cellulose nanofibers. Ind Eng Chem Res 59(23):10904–10913. https://doi.org/10.1021/acs.iecr.0c01053

16. Chirayil CJ, Joy J, Mathew L, Mozetic M, Koetz J, Thomas S (2014) Isolation and characterization of cellulose nanofibrils from Helicteres isora plant. Ind Crops Prod 59:27–34. https://doi.org/10.1016/j.indcrop.2014.04.020

17. Ramadevi P, Sampathkumar D, Srinivasa CV, Bennehalli B (2012) Effect of alkali treatment on water absorption of single cellulosic abaca fiber. BioResources 7(3):3515–3524. https://doi.org/10.15376/biores.7.3.3515-3524

18. Rizwan M, Gilani SR, Durrani AI, Naseem S (2021) Low temperature green extraction of Acer platanoides cellulose using nitrogen protected microwave assisted extraction (NPMAE) technique. Carbohydr Polym 272:118465. https://doi.org/10.1016/j.carbpol.2021.118465

19. Segal LGJMA, Creely JJ, Jr M, A. E., Conrad CM (1959) An empirical method for estimating the degree of crystallinity of native cellulose using the X-ray diffractometer. Text Res J 29(10):786–794

20. Raju V, Revathiswaran R, Subramanian KS, Parthiban KT, Chandrakumar K, Anoop EV, Chirayil CJ (2023) Isolation and characterization of nanocellulose from selected hardwoods, viz., Eucalyptus tereticornis Sm. And Casuarina equisetifolia L., by steam explosion method. Sci Rep 13(1). https://doi.org/10.1038/s41598-022-26600-5

21. Zhao G, Du J, Chen W, Pan M, Chen D (2019) Preparation and thermostability of cellulose nanocrystals and nanofibrils from two sources of biomass: rice straw and poplar wood. Cellulose 26(16):8625–8643. https://doi.org/10.1007/s10570-019-02683-8

22. Mrudhula R, Reddy DS, P., Veeresh Kumar GB (2023) Preparation of cellulose nanofibers (CNFs) from Cajanus cajan (pigeon pea) and Acacia arabica (Babul plant). In B. B. V. L. Deepak, M. V. A. R. Bahubalendruni, D. R. K. Parhi, & B. Biswal (Eds.), *Recent Trends in Product Design and Intelligent Manufacturing Systems* (pp. 429–438). Springer Nature. https://doi.org/10.1007/978-981-19-4606-6_40

23. Gond RK, Gupta MK, Jawaid M (2021) Extraction of nanocellulose from sugarcane bagasse and its characterization for potential applications. Polym Compos 42(10):5400–5412. https://doi.org/10.1002/pc.26232

24. Verma YK, Singh AK, Paswan MK, Sonker PK (2023) Importance of functionalized jute fibers in the field of nano cellulose for the preparation of biodegradable nano composites. *Materials Today: Proceedings*, *80*, 254–257. https://doi.org/10.1016/j.matpr.2023.01.031

25. Syafri E, Kasim A, Abral H, Asben A (2018) Cellulose nanofibers isolation and characterization from ramie using a chemical-ultrasonic treatment. J Nat Fibers. https://doi.org/10.1080/15440478.2018.1455073

26. Wu Q, Ding C, Wang B, Rong L, Mao Z, Feng X (2024) Green, chemical-free, and high-yielding extraction of nanocellulose from waste cotton fabric enabled by electron beam irradiation. Int J Biol Macromol 267:131461. https://doi.org/10.1016/j.ijbiomac.2024.131461

27. Padzil FNM, Lee SH, Ainun ZMAA, Lee CH, Abdullah LC (2020) Potential of oil palm empty fruit bunch resources in nanocellulose hydrogel production for versatile applications: a review. Materials 13(5):1245. https://doi.org/10.3390/ma13051245

28. Balakrishnan P, Gopi S, Geethamma VG, Kalarikkal N, Thomas S (2018), August Cellulose nanofiber vs nanocrystals from pineapple leaf fiber: a comparative studies on reinforcing efficiency on starch nanocomposites. In Macromolecular Symposia (Vol. 380, No. 1, p. 1800102). https://doi.org/10.1002/masy.201800102

29. Wu J, Du X, Yin Z, Xu S, Xu S, Zhang Y (2019) Preparation and characterization of cellulose nanofibrils from coconut coir fibers and their reinforcements in biodegradable composite films. Carbohydr Polym 211:49–56. https://doi.org/10.1016/j.carbpol.2019.01.093

30. Naseem S, Durrani AI, Rizwan M, Yasmeen F, Siddiqui S, Habib F (2024) Sono-microwave assisted chlorine free and ionic liquid (SMACIL) extraction of cellulose from Urtica dioica: a benign to green approach. Int J Biol Macromol 259:129059. https://doi.org/10.1016/j.ijbiomac.2023.129059

31. Rizwan M, Gilani SR, Durrani AI, Naseem S (2021) Cellulose extraction of Alstonia scholaris: a comparative study on efficiency of different bleaching reagents for its isolation and characterization. Int J Biol Macromol 191:964–972. https://doi.org/10.1016/j.ijbiomac.2021.09.155

32. Tenaye T, Mohammed SA, Jabasingh SA (2022) Sustainable synthesis and characterization of Enset cellulose nanocrystals (E-CNp) from Enset Ventricosum biomass and its application in the fabrication of Enset cellulose nanocomposite (E-CNc). Biomass Convers Biorefinery 1–16. https://doi.org/10.1007/s13399-022-02682-z

33. Baskaran PG, Kathiresan M, Senthamaraikannan P, Saravanakumar SS (2018) Characterization of new natural cellulosic fiber from the bark of dichrostachys cinerea. J Nat Fibers 15(1):62–68. https://doi.org/10.1080/15440478.2017.1304314

34. Umashankaran M, Gopalakrishnan S (2019) Characterization of bio-fiber from Pongamiapinnata L. Bark as possible reinforcement of polymer composites. Journal of natural fibers

35. Hussin FNNM, Attan N, Wahab RA (2020) Extraction and characterization of nanocellulose from raw oil palm leaves (Elaeis guineensis). Arab J Sci Eng 45:175–186. https://doi.org/10.1007/s13369-019-04131-y

36. Scarano D, Galletto P, Lamberti C, De Franceschi R, Zecchina A (1997) Morphology and CO adsorptive properties of CuCl polycrystalline films: a SEM and FTIR study. Surf Sci 387(1–3):236–242. https://doi.org/10.1016/S0039-6028(97)00359-2

37. Nishiyama Y, Sugiyama J, Chanzy H, Langan P (2003) Crystal structure and hydrogen bonding system in cellulose I α from synchrotron X-ray and neutron fiber diffraction. J Am Chem Soc 125(47):14300–14306. https://doi.org/10.1021/ja037055w

38. Leong, S. L., Tiong, S. I. X., Siva, S. P., Ahamed, F., Chan, C. H., Lee, C. L., …Ho, Y. K. (2022). Morphological control of cellulose nanocrystals via sulfuric acid hydrolysis based on sustainability considerations: an overview of the governing factors and potential challenges. J Environ Chem Eng 10(4), 108145. https://doi.org/10.1016/j.jece.2022.108145

39. Dhali K, Daver F, Cass P, Adhikari B (2021) Isolation and characterization of cellulose nanomaterials from jute bast fibers. J Environ Chem Eng 9(6):106447. https://doi.org/10.1016/j.jece.2021.106447

40. Brito BS, Pereira FV, Putaux JL, Jean B (2012) Preparation, morphology and structure of cellulose nanocrystals from bamboo fibers. Cellulose 19:1527–1536. https://doi.org/10.1007/s10570-012-9738-9

41. Xie J, Qi J, Hu T, De Hoop CF, Hse CY, Shupe TF (2016) Effect of fabricated density and bamboo species on physical–mechanical properties of bamboo fiber bundle reinforced composites. J Mater Sci 51:7480–7490. https://doi.org/10.1007/s10853-016-0024-3

42. Kusmono K, Akbar DA (2020) Influence of hydrolysis conditions on characteristics of nanocrystalline cellulose extracted from ramie fibers by. https://doi.org/10.21203/rs.3.rs-31322/v1. Hydrochloric Acid Hydrolysis

43. Meng F, Wang G, Du X, Wang Z, Xu S, Zhang Y (2019) Extraction and characterization of cellulose nanofibers and nanocrystals from liquefied banana pseudo-stem residue. Compos Part B: Eng 160:341–347. https://doi.org/10.1016/j.compositesb.2018.08.048

44. Valencia L, Arumughan V, Jalvo B, Maria HJ, Thomas S, Mathew AP (2019) Nanolignocellulose extracted from environmentally undesired Prosopis juliflora. ACS Omega 4(2):4330–4338. https://doi.org/10.1021/acsomega.8b02685

45. do Nascimento, D. M., Almeida, J. S., Vale, M. D. S., Leitão, R. C., Muniz, C. R.,de Figueirêdo, M. C. B., … Rosa, M. D. F. (2016). A comprehensive approach for obtaining cellulose nanocrystal from coconut fiber. Part I: Proposition of technological pathways.Industrial Crops and Products, 93, 66–75. https://doi.org/10.1016/j.indcrop.2015.12.078

46. Deepa, B., Abraham, E., Cordeiro, N., Mozetic, M., Mathew, A. P., Oksman, K., … Pothan,L. A. (2015). Utilization of various lignocellulosic biomass for the production of nanocellulose: a comparative study. Cellulose, 22, 1075–1090. https://doi.org/10.1007/s10570-015-0554-x

47. George CSJC, N., Narayanankutty SK (2016) Isolation and characterization of cellulose nanofibrils from arecanut husk fibre. Carbohydr Polym 142:158–166. https://doi.org/10.1016/j.carbpol.2016.01.015

48. Trache D, Tarchoun AF, Derradji M, Hamidon TS, Masruchin N, Brosse N, Hussin MH (2020) Nanocellulose: from fundamentals to advanced applications. Front Chem 8:392. https://doi.org/10.3389/fchem.2020.00392

49. Khouri S (2010) Experimental characterization and theoretical calculations of responsive polymeric systems (Master's thesis, University of Waterloo)

50. Pelissari FM, Sobral PJ do A., Menegalli FC (2014) Isolation and characterization of cellulose nanofibers from banana peels. Cellulose, 21(1), 417–432. https://doi.org/10.1007/s10570-013-0138-6